Energy relaxation in dense, strongly coupled two-temperature plasmas

J. Vorberger and D. O. Gericke
Centre for Fusion, Space and Astrophysics, Department of Physics, University of Warwick, Coventry CV4 7Al, United Kingdom

Th. Bornath
Institut für Physik, Universität Rostock, 18051 Rostock, Germany

M. Schlanges
Institut für Physik, Ernst-Moritz-Arndt-Universität Greifswald, 17489 Greifswald, Germany

(Received 25 November 2009; revised manuscript received 1 March 2010; published 28 April 2010)

A quantum kinetic approach for the energy relaxation in strongly coupled plasmas with different electron and ion temperatures is presented. Based on the density operator formalism, we derive a balance equation for the energies of electrons and ions connecting kinetic, correlation, and exchange energies with a quite general expression for the electron-ion energy-transfer rate. The latter is given in terms of the correlation function of density fluctuations which allows for a derivation of increasingly realistic approximation schemes including a coupled-mode expression. The equilibration of the contributions of the total energy including the species temperatures in dense hydrogen and beryllium relevant for inertial confinement fusion is investigated as an example.

DOI: 10.1103/PhysRevE.81.046404 PACS number(s): 52.25.Dg, 52.25.Kn, 52.27.Gr

I. INTRODUCTION

The experimental characterization of strongly coupled plasmas and warm dense matter becomes increasingly accurate with the development of new methods for the creation and probing of such states. For instance, x-ray scattering allows not only for the measurement of the equation of state but also to obtain structural, dynamic, and collective properties of dense matter [1–5]. Moreover, traditional shock [6,7] and isentropic compression experiments [8,9] keep extending the parameter space tested. With these new possibilities, one is now able to probe the physics of high-energy density matter as it is encountered during inertial confinement fusion [10] or in the interior of planets [11,12].

The creation of states with high energy density in the laboratory requires a large and fast energy input into matter. Since static techniques, such as diamond anvil cells, are restricted to lower temperatures and densities, one relies on dynamic experiments applying intense particle beams or lasers to heat and compress the material under investigation. Inevitably, highly nonequilibrium states are produced with the energy being pumped mainly into either the ion or the electron subsystem.

Nonequilibrium states are of great interest by itself as they reveal many dynamic and collective properties of the system more clearly. However, a good understanding of the relaxation processes driven by the initial energy deposition is also needed for definitive measurements of equilibrium properties. Apart from the hydrodynamic response, temperature equilibration takes the longest of all relaxation processes and, thus, defines the minimum time delay between pump and probe pulses needed for equilibrium measurements.

Temperature equilibration is furthermore interesting since its time scale of a few picoseconds is experimentally accessible [4,5,13]. However, an intense discussion about relaxation times started when Dharma-wardana and Perrot [14] found considerably smaller energy-transfer rates as predicted by the Landau-Spitzer (LS) theory [15,16] and early computer simulations [17,18]. Indeed, experiments investigating dense plasmas found also strong indications of longer relaxation times, thus smaller energy-transfer rates [19–21].

Two shortcomings of the easy-to-use LS approach were associated with these discrepancies: (i) the neglect of the collective excitations in the plasma and (ii) the use of classical collisions in a (unscreened) Coulomb field. The latter was investigated applying a quantum approach for binary collisions which yields however even larger energy-transfers rates [22–24]. Considering independent electron and ion modes within Fermi's golden rule (FGR) yields rates very close to the LS results [25,26]. The coupling of the electron and ion modes can however change the mode structure and consequently the effective electron-ion interaction. Such coupling effects are also known for electron-phonon systems in semiconductors [27,28]. For a more realistic description of temperature equilibration, it is thus essential to develop a theory that includes the collective modes of the fully coupled electron-ion system.

Rigorous descriptions of temperature relaxation not only consider the energy-transfer rates but also involve the interplay of all contributions to the internal energy. In addition to the kinetic parts, which define the species temperatures, correlations and exchange energies [29–32] and the ionization equilibrium [33–35] can considerably influence the relaxation process.

Here, we assume ionization, recombination, and charge-transfer processes to be completed and concentrate on the electron-ion energy relaxation including collective modes and correlation energies in a fully coupled system. We use a quantum kinetic description which avoids any *ad hoc* cutoffs known from classical descriptions and enables us to rigorously derive balance equations and formulas for the energy-transfer rates in two-temperature plasmas. Thus, a consistent description of temperature changes, heat capacities, and energy transfer is developed.

In Sec. II, general energy balance equations for multicomponent systems are derived. This approach allows for considering correlations in both the internal energies and the energy-transfer rates. Interestingly, it follows that the electron-ion cross term in the interaction energy contributes equally to the energies of the electrons and ions.

Section III demonstrates how known expressions for the energy-transfer rates, namely the FGR and CM rates, follow from the presented formalism. It is shown that these rates describe the transfer of total energy between the subsystems and the approximations made are highlighted. As the effects of coupled collective modes are still under discussion [14,36–40], we present a few examples for the electron-ion energy-transfer rates.

In Sec. IV, we show the temperature evolution in dense, fully coupled systems including quantum effects and nonideality contributions. We find deviations from an ideal temperature relaxation and demonstrate how correlations and collective modes affect the shape of the temperature curves, the relaxation time, and the final temperature. It turns out that the most important effect of coupled modes (CMs) is not an increase in relaxation time but a different form of the time evolution of the electron and ion temperatures, while correlations mainly affect the final plasma temperature. A comparison with recent molecular-dynamics (MD) simulations [41] shows rather good agreement for the electron-ion energy transfer of the nearly classical system considered but small deviations in the final temperature due to quantum effects.

II. ENERGY BALANCE EQUATION

In kinetic theory, one usually derives balance equations starting from a specific kinetic equation. This approach makes it particularly difficult to incorporate contributions to the potential energy. Here, we choose another way by starting from the definitions of kinetic and potential energies in terms of reduced density operators and using their equations of motion, the Born-Bogoliubov-Green-Kirkwood-Yvon (BBGKY) hierarchy. Afterwards approximations, which allow generalization of the results of standard kinetic theory, will be introduced.

To describe energy relaxation, we derive a balance equation for the total energy of spatially homogeneous plasmas consisting of electrons with density n_e and ions in a charge state Z with densities n_Z. Electrons and ions are both considered to have established well-defined but different temperatures.

The mean kinetic and the potential energies of species 'a' are defined by

$$\langle K_a(t)\rangle = \mathrm{Tr}_1\{\hat{H}_a\hat{\rho}_a(t)\}, \tag{1}$$

$$\langle V_a(t)\rangle = \frac{1}{2}\sum_b \mathrm{Tr}_{1,2}\{\hat{V}_{ab}\hat{\rho}_{ab}(t)\}, \tag{2}$$

where $\hat{\rho}_a$ and $\hat{\rho}_{ab}$ are the one- and two-particle density operators. The traces are performed over one- and two-particle spaces with respect to vectors $|1\rangle$ and $|2\rangle$ in the respective state spaces for particles a and b. Note that the electron-ion cross term is here split equally between electron and ion energies. The density operators are determined by their equation of motion which are the first two equations of the quantum version of the BBGKY hierarchy [42]

$$i\hbar\frac{\partial}{\partial t}\hat{\rho}_a = [\hat{H}_a,\hat{\rho}_a] + \sum_b \mathrm{Tr}_2[\hat{V}_{ab},\hat{\rho}_{ab}], \tag{3}$$

$$i\hbar\frac{\partial}{\partial t}\hat{\rho}_{ab} = [\hat{H}_{ab},\hat{\rho}_{ab}] + \sum_c \mathrm{Tr}_3[(\hat{V}_{ac}+\hat{V}_{bc}),\hat{\rho}_{abc}]. \tag{4}$$

Here, the square brackets denote the commutator, that is $[\hat{A},\hat{B}]=\hat{A}\hat{B}-\hat{B}\hat{A}$.

Using the first equation, we find for the change in the mean kinetic energy of species a,

$$\frac{\partial}{\partial t}\langle K_a\rangle = \frac{1}{i\hbar}\sum_b \mathrm{Tr}_{1,2}\hat{H}_a[\hat{V}_{ab},\hat{\rho}_{ab}] \tag{5}$$

as the contribution following from the first term at the right-hand side (rhs) of Eq. (3) vanishes due to the cyclical invariance of the trace. For further considerations, we rewrite Eq. (5) in the form

$$\frac{\partial}{\partial t}\langle K_a\rangle = \frac{1}{2i\hbar}\sum_b \mathrm{Tr}_{1,2}\{(\hat{H}_a+\hat{H}_b)[\hat{V}_{ab},\hat{\rho}_{ab}]\} + \frac{1}{2i\hbar}\sum_b \mathrm{Tr}_{1,2}\{(\hat{H}_a-\hat{H}_b)[\hat{V}_{ab},\hat{\rho}_{ab}]\}. \tag{6}$$

The first term on the rhs can be transformed using Eq. (4) for the two-particle density operator. Furthermore, we define $\hat{H}_a+\hat{H}_b=\hat{H}^0_{ab}$, and it holds that $\mathrm{Tr}\,\hat{A}[\hat{B},\hat{C}]=-\mathrm{Tr}\,\hat{B}[\hat{A},\hat{C}]$. Then, we obtain

$$\frac{1}{2}\sum_b \mathrm{Tr}_{1,2}\frac{1}{i\hbar}\{\hat{V}_{ab}[\hat{H}^0_{ab},\hat{\rho}_{ab}]\} = \frac{\partial}{\partial t}\frac{1}{2}\sum_b \mathrm{Tr}_{1,2}\{\hat{V}_{ab}\hat{\rho}_{ab}\} - \frac{1}{2i\hbar}\sum_b \mathrm{Tr}_{1,2}\{\hat{V}_{ab}[\hat{V}_{ab},\hat{\rho}_{ab}]\} - \frac{1}{2i\hbar}\sum_{b,c} \mathrm{Tr}_{1,2,3}\{\hat{V}_{ab}[(\hat{V}_{ac}+\hat{V}_{bc}),\hat{\rho}_{abc}]\}. \tag{7}$$

The first term on the rhs is the time derivative of the mean potential energy [cf. Eq. (2)]. The other two terms vanish due to the properties of the traces performed over two- and three-particle space, respectively. Equation (6) can then be cast into

$$\frac{\partial}{\partial t}\langle K_a\rangle + \frac{\partial}{\partial t}\langle V_a\rangle = \sum_b Z_{ab}, \tag{8}$$

which connects changes in the kinetic energy with the time derivative of the mean potential energy $\langle V_a\rangle$ of species a, and the energy-transfer rate between species a and b given by

$$Z_{ab} = \frac{1}{2i\hbar}\mathrm{Tr}_{1,2}\{(\hat{H}_a - \hat{H}_b)[\hat{V}_{ab},\hat{\rho}_{ab}]\}. \tag{9}$$

Note that only terms with $b \neq a$ give nonzero rates and that $Z_{ab}=-Z_{ba}$ holds. Summation over species a in Eq. (8) thus gives

$$\sum_a \frac{\partial}{\partial t}\langle K_a\rangle + \sum_a \frac{\partial}{\partial t}\langle V_a\rangle = \sum_{a,b} Z_{ab} = 0, \tag{10}$$

which expresses the conservation of total energy.

III. ENERGY-TRANSFER RATE

Expression (9) for the energy-transfer rate between the species is not suitable for evaluation. Here, we first derive a general formula in terms of the correlation function of density fluctuations and then show how approximate forms can be derived from that general expression.

A. General expressions

We write the energy-transfer rate in the form

$$Z_{ab} = \frac{1}{2i\hbar}\mathrm{Tr}_{1,2}\{(\hat{H}_a - \hat{H}_b)[\hat{V}_{ab},\hat{\rho}_a\hat{\rho}_b + \hat{\rho}_{ab}^{\mathrm{corr}}]\}, \tag{11}$$

where $\hat{\rho}_{ab}^{\mathrm{corr}}$ denotes the correlation part of the two-particle density operator $\hat{\rho}_{ab}$. The density matrix of $\hat{\rho}_{ab}$ in position space can be written as

$$\langle 12|\hat{\rho}_{ab}(t)|2'1'\rangle = \langle \psi_a^\dagger(1',t)\psi_b^\dagger(2',t)\psi_b(2,t)\psi_a(1,t)\rangle, \tag{12}$$

with the creation and annihilation operators of each species $\psi_a^\dagger$ and ψ_a, respectively. Spin variables will be suppressed for simplicity.

Our goal is to derive expressions for the energy-transfer rate for dense multi-temperature plasmas including the important contributions of collective excitations. For this purpose, it is useful to apply the relation $(b \neq a)$

$$\langle 12|\hat{\rho}_{ab}^{\mathrm{corr}}(t)|2'1'\rangle = i\hbar L_{ab}^<(11't,22't')|_{t=t'}, \tag{13}$$

which connects the correlation part of the density matrix with the correlation function of density fluctuations $L_{ab}^<$. The latter is given by

$$\begin{aligned} i\hbar L_{ab}^<(11't_1,22't_2) = {} & \langle \psi_b^\dagger(2',t_2)\psi_b(2,t_2)\psi_a^\dagger(1',t_1)\psi_a(1,t_1)\rangle \\ & - \langle \psi_b^\dagger(2',t_2)\psi_b(2,t_2)\rangle\langle \psi_a^\dagger(1',t_1)\psi_a(1,t_1)\rangle. \end{aligned} \tag{14}$$

Applying Eq. (13) and the equations of motion for the function $L_{ab}^<(t,t')$, one can derive the following expression for the energy-transfer rate (see the Appendix for details):

$$Z_{ab} = -\hbar\,\mathrm{Tr}_{1,2}\int_{-\infty}^{\infty}\frac{d\omega}{2\pi}\omega\hat{V}_{ab}L_{ab}^<(12;\omega,t). \tag{15}$$

Here $L_{ab}^<(12;\omega,t)$ is the Fourier transform of $L_{ab}^<(1t_1,2t_2)$ with respect to the difference time $\tau=t_1-t_2$ and the macroscopic time is given by $t=\frac{1}{2}(t_1+t_2)$. If we further account for the fact that the function $iL_{ab}^<(1t_1,2t_2)$ is real and, therefore, $iL_{ab}^<(12;\omega,t)$ has an even real part and an odd imaginary part, the energy-transfer rate can be written as

$$Z_{ab} = -2\,\mathrm{Im}\,\mathrm{Tr}_{1,2}\int_0^\infty\frac{d\omega}{2\pi}\omega V_{ab}\;\; i\hbar L_{ab}^<(12;\omega,t). \tag{16}$$

Using the position space for the evaluation of the trace and introducing the Fourier transform with respect to the relative variable $\mathbf{r}=\mathbf{r}_1-\mathbf{r}_2$, the rate Z_{ab} for spatially homogeneous systems (no dependence on $\mathbf{R}=\frac{1}{2}[\mathbf{r}_1+\mathbf{r}_2]$) takes finally the form

$$Z_{ab} = -2\mathcal{V}\,\mathrm{Im}\int\frac{d^3\mathbf{q}}{(2\pi\hbar)^3}\int_0^\infty\frac{d\omega}{2\pi}\omega V_{ab}(q)i\hbar L_{ab}^<(\mathbf{q};\omega,t), \tag{17}$$

where $\mathcal{V}$ denotes the volume. Thus, the rate of energy transfer between species a and b is determined by the Fourier transform of the correlation function of density fluctuations $L_{ab}^<(\mathbf{q};\omega,t)$. The property $Z_{ab}=-Z_{ba}$ can be shown using the relation $L_{ab}^<(\omega,t)=L_{ba}^<(-\omega,t)$.

B. Equations for the function L_{ab}

Appropriate approximation schemes for the correlation function of density fluctuations $L_{ab}^<$ are required before expression (17) can be applied to determine the energy-transfer rate. $L_{ab}^<$ is defined in the particle-hole channel and is a special case of the function L_{ab}. Thus, we start from the equation for the function L_{ab} defined on the Keldysh time contour [43,44]

$$L_{ab}(t_1,t_2) = \Pi_{ab}(t_1,t_2) + \sum_{c,d}\int_{\mathcal{C}} d\bar{t}\,\Pi_{ac}(t_1,\bar{t})V_{cd}L_{db}(\bar{t},t_2). \tag{18}$$

Here, Π_{ab} is the polarization function, V_{ab} is the Coulomb potential, and the symbol $\int_{\mathcal{C}}$ stands for the integration along the Keldysh contour. For simplicity, only the time variables were given explicitly. Applying the well-known techniques originally introduced by Keldysh, equations for the correlation functions $L_{ab}^{\gtrless}$, and for the causal and anticausal functions L_{ab}^c and L_{ab}^a can be obtained from Eq. (18) [43,44]. Furthermore, the equations for the retarded and advanced functions follow easily.

Now we will specify our considerations for a two-component plasma consisting of electrons and ions. As a first approximation, we assume that $\Pi_{ab}=\delta_{ab}\Pi_a$ where Π_a is the polarization function of the subsystem containing species a. Correlation effects within the subsystems will be included via local-field corrections (see below). The inclusion of cross correlations between the species in Π_{ab} is nowadays not feasible.

Applying this approximation, we have the following system of equations defined on the contour:

$$L_{ee} = \Pi_e + \Pi_e V_{ee}L_{ee} + \Pi_e V_{ei}L_{ie},$$

$$L_{ei} = \Pi_e V_{ee}L_{ei} + \Pi_e V_{ei}L_{ii},$$

$$L_{ie} = \Pi_i V_{ie} L_{ee} + \Pi_i V_{ii} L_{ie},$$

$$L_{ii} = \Pi_i + \Pi_i V_{ie} L_{ei} + \Pi_i V_{ii} L_{ii}. \tag{19}$$

Here, we used a compact form where all variables are suppressed; in the time domain, the equations have the same integral structure as Eq. (18). It is now useful to introduce two auxiliary functions, $\mathcal{L}_e$ and $\mathcal{L}_i$, defined by

$$\mathcal{L}_a = \Pi_a + \Pi_a V_{aa} \mathcal{L}_a, \tag{20}$$

which describe subsystems containing only electrons or ions. Then the equation for L_{ei} takes the form

$$L_{ei} = \mathcal{L}_e V_{ei} \mathcal{L}_i + \mathcal{L}_e V_{ei} \mathcal{L}_i V_{ie} L_{ei} = \mathcal{P}_{ei} + \mathcal{P}_{ei} V_{ei} L_{ei}, \tag{21}$$

with the definition $\mathcal{P}_{ei} = \mathcal{L}_e V_{ei} \mathcal{L}_i$. Again, Eq. (21) has to be considered on the Keldysh contour.

The equation for the correlation function $L_{ei}^<$ on the physical time axis can be obtained from Eq. (21) using the Langreth-Wilkins rules [45]

$$L_{ei}^<(t_1,t_2) = \mathcal{P}_{ei}^<(t_1,t_2) + \int_{-\infty}^{+\infty} d\bar{t}\, \mathcal{P}_{ei}^<(t_1,\bar{t}) V_{ie} L_{ei}^A(\bar{t},t_2) + \int_{-\infty}^{+\infty} d\bar{t}\, \mathcal{P}_{ei}^R(t_1,\bar{t}) V_{ie} L_{ei}^<(\bar{t},t_2). \tag{22}$$

The advanced density response function L_{ei}^A needed here is determined by

$$L_{ei}^A(t_1,t_2) = \mathcal{P}_{ei}^A(t_1,t_2) + \int_{-\infty}^{+\infty} d\bar{t}\, \mathcal{P}_{ei}^A(t_1,\bar{t}) V_{ie} L_{ei}^A(\bar{t},t_2) \tag{23}$$

and the retarded function, e.g., L_{ei}^R, satisfies an equation of the same form. From the definition $\mathcal{P}_{ei} = \mathcal{L}_e V_{ei} \mathcal{L}_i$, we find that the equations for the quantities $\mathcal{P}_{ei}^<$, $\mathcal{P}_{ei}^R$, and $\mathcal{P}_{ei}^A$ have similar structures as Eqs. (22) and (23), respectively.

Again, we introduce difference and sum variables, i.e., $\tau = t_1 - t_2$, $t = \frac{1}{2}(t_1 + t_2)$, $\mathbf{r} = \mathbf{r}_1 - \mathbf{r}_2$, and $\mathbf{R} = \frac{1}{2}(\mathbf{r}_1 + \mathbf{r}_2)$, and apply a gradient expansion where we only account for the terms of lowest order with respect to the variables t and $\mathbf{R}$ [44]. In spatially homogeneous plasmas, there is no dependence on $\mathbf{R}$. After Fourier transformation with respect to the difference variables, Eqs. (22) and (23) become a set of algebraic equations for functions with the variables $\mathbf{q}$, ω, and t. To get a compact representation, we suppress these variables again. For $L_{ei}^< \hat{=} L_{ei}^<(\mathbf{q};\omega,t)$ it then follows that

$$\begin{aligned} L_{ei}^< &= \mathcal{P}_{ei}^< + \mathcal{P}_{ei}^< V_{ie} L_{ei}^A + \mathcal{P}_{ei}^R V_{ie} L_{ei}^< \\ &= (1 + L_{ei}^R V_{ie}) \mathcal{P}_{ei}^< (1 + V_{ie} L_{ei}^A) \\ &= \frac{1}{1 - \mathcal{P}_{ei}^R V_{ie}} \mathcal{P}_{ei}^< \frac{1}{1 - V_{ie} \mathcal{P}_{ei}^A}, \end{aligned} \tag{24}$$

where $\mathcal{P}_{ei}^< = \mathcal{L}_e^< V_{ei} \mathcal{L}_i^A + \mathcal{L}_e^R V_{ei} \mathcal{L}_i^<$. In the second step, we have used the relation $L_{ei}^{R/A} = \mathcal{P}_{ei}^{R/A} / (1 - \mathcal{P}_{ei}^{R/A} V_{ie})$. With $\mathcal{P}_{ei}^{R/A} = \mathcal{L}_e^{R/A} V_{ei} \mathcal{L}_i^{R/A}$, we finally obtain

$$L_{ei}^<(\mathbf{q};\omega,t) = \frac{\mathcal{P}_{ei}^<(\mathbf{q};\omega,t)}{|1 - \mathcal{L}_e^R(\mathbf{q};\omega,t) V_{ei}(q) \mathcal{L}_i^R(\mathbf{q};\omega,t) V_{ie}(q)|^2}. \tag{25}$$

C. Fermi golden rule formula

Assuming weak coupling between electrons and ions, the correlation function $L_{ei}^<$ can be approximated by the first term in the first line of Eq. (24)

$$L_{ei}^<(\mathbf{q};\omega,t) \approx \mathcal{P}_{ei}^<(\mathbf{q};\omega,t). \tag{26}$$

Inserting this approximation into the general expression for the energy-transfer rate (17) yields

$$Z_{ei}(t) = -2\mathcal{V}\, \mathrm{Im} \int \frac{d^3\mathbf{q}}{(2\pi\hbar)^3} \int_0^\infty \frac{d\omega}{2\pi} \omega V_{ei}(q) i\hbar [\mathcal{L}_e^<(\mathbf{q};\omega,t) \times V_{ei}(q) \mathcal{L}_i^A(\mathbf{q};\omega,t) + \mathcal{L}_e^R(\mathbf{q};\omega,t) V_{ei}(q) \mathcal{L}_i^<(\mathbf{q};\omega,t)]. \tag{27}$$

As we consider systems with well-defined temperatures for each species, the correlation functions for every subsystem $\mathcal{L}_a^<$ can be expressed in terms of the spectral and Bose functions

$$i\mathcal{L}_a^<(\mathbf{q};\omega,t) = \mathcal{A}_a(\mathbf{q};\omega,t;T_a) n_B(\omega/T_a) \tag{28}$$

where

$$\mathcal{A}_a(\mathbf{q};\omega,t;T_a) = -2\, \mathrm{Im}\, \mathcal{L}_a^R(\mathbf{q};\omega,t;T_a) \tag{29}$$

and $n_B(\omega/T_a) = [\exp(\hbar\omega/k_B T_a) - 1]^{-1}$. Applying these relations to the electron-ion energy transfer yields

$$Z_{ei}(t) = -\mathcal{V}\hbar \int \frac{d^3\mathbf{q}}{(2\pi\hbar)^3} \int_0^\infty \frac{d\omega}{2\pi} \omega |V_{ei}(q)|^2 \times \mathcal{A}_e(\mathbf{q};\omega,t) \mathcal{A}_i(\mathbf{q};\omega,t) \Delta N_B(\omega), \tag{30}$$

where we introduced $\Delta N_B(\omega) = n_B(\omega/T_e) - n_B(\omega/T_i)$. This expression agrees with the FGR formula derived by Dharma-wardana and Perrot [14]. It is fully determined by the independent spectral functions of the electron and ion subsystems. In our derivation, this decoupling originates in approximation (26). Although being derived in lowest order, expression (30) has a number of advantages compared to the LS approach: (i) it is a rate for the total-energy transfer, not only the kinetic contributions; (ii) it is fully quantum mechanically which avoids arbitrary cutoffs; and (iii) it allows for the incorporation of strong coupling within the subsystems.

Strong coupling within a subsystem can be accounted for by local-field corrections (LFCs). Using static local-field corrections, the retarded density response functions can be written as

$$\mathcal{L}_a^R(\mathbf{q};\omega,t) = \frac{\Pi_a^0(\mathbf{q};\omega,t)}{1 - V_{aa}(q)[1 - G_a(\mathbf{q},t)] \Pi_a^0(\mathbf{q};\omega,t)}. \tag{31}$$

Here, Π_a^0 is the polarization function in the random phase approximation (RPA)

$$\Pi_a^0(\mathbf{q};\omega,t) = \int \frac{d\mathbf{p}}{(2\pi\hbar)^3} \frac{f_a(\mathbf{p},t) - f_a(\mathbf{p}+\mathbf{q},t)}{\hbar\omega + \epsilon_a(\mathbf{p}) - \epsilon_a(\mathbf{p}+\mathbf{q}) + i\varepsilon}, \tag{32}$$

where f_a is the distribution function of the particles in the subsystem a in local equilibrium with temperature T_a. The local-field factor G_a is connected to the static structure factor $S_{aa}(\mathbf{q},t)$ via [46]

$$G_a(\mathbf{q},t) = 1 - \frac{k_B T_a}{n_a V_{aa}(q)} \left(\frac{1}{S_{aa}(\mathbf{q},t)} - 1 \right). \tag{33}$$

D. Coupled mode expression

Approximation (26) leading to FGR formula (30) has to be avoided for a description of coupled modes. For such generalization, we consider the full expression for $L_{ei}^{<}$ as in Eq. (25) in energy-transfer rate (17). Again, we write the density response in terms of spectral functions using Eqs. (28) and (29) and arrive at

$$Z_{ei}(t) = -\mathcal{V}\hbar \int \frac{d^3\mathbf{q}}{(2\pi\hbar)^3} \int_0^\infty \frac{d\omega}{2\pi} \omega |V_{ei}(q)|^2 \times \frac{\mathcal{A}_e(\mathbf{q};\omega,t)\mathcal{A}_i(\mathbf{q};\omega,t)\Delta N_B(\omega)}{|1 - \mathcal{L}_e^R(\mathbf{q};\omega,t)\mathcal{L}_i^R(\mathbf{q};\omega,t)V_{ei}^2(q)|^2}. \tag{34}$$

This equation has the same structure as that given in Ref. [14] when coupled collective modes are considered. CM expression (34) and FGR formula (30) differ by the denominator which describes the coupling of ion and electron modes in two-temperature plasmas. This becomes clear if one recognizes that both functions $\mathcal{A}_e$ and $\mathcal{A}_i$ are renormalized by this denominator which contains the electron and the ion responses. As a result, the ion modes in the CM description are screened and become acoustic, whereas in the FGR approach an ion plasmon mode exists [40].

Another important difference between the FGR and CM description is how strong-coupling effects modify the results. Within FGR, the ionic response can often be treated analytically: the ω integral in Eq. (30) can be performed using the f-sum rule for the ionic response function [25,26]. In this case, the ionic correlations are accounted for without the need of an explicit calculation of $G_i(q,t)$, and the full FGR result agrees with the one in RPA. Thus, strong coupling does not affect the FGR result. Such a treatment is not possible within the CM approach. Here, the full, two-component mode structure must be calculated and integrated numerically. Coupled collective modes have been shown to significantly reduce the electron-ion energy transfer even for weak coupling [40]. Naturally, strong coupling affects the occurrence, the position, and the width of the ion acoustic modes and, therefore, can further change the energy-transfer rates. Indeed, ionic LFCs play the most important role as the ions are usually the most strongly coupled species. Here, we include ionic LFCs via the connection to the static structure factor (33) where the latter is calculated with the hypernetted-chain method (see, e.g., Refs. [47,48]).

We want to recall the approximations applied during the derivation of Eq. (34): first, the polarization function was used in a diagonal form, i.e., $\Pi_{ab} = \delta_{ab}\Pi_a$, where Π_a is restricted to the contributions coming from species a. Thus, Π_a is the polarization function of the subsystem of species a. Second, only the lowest-order term in the gradient expansion with respect to the macroscopic time t is considered as the subsystems are assumed to be in local equilibrium with temperature T_a [44,45].

Again, the key quantities in Eq. (34) are the density response functions of the subsystems given by Eq. (31). For numerical calculations, it is more convenient to write the CM formula (34) in a different form. From Eq. (20) it follows that

$$\mathcal{L}_a^R(\mathbf{q};\omega,t) = \frac{\Pi_a^R(\mathbf{q};\omega,t)}{1 - \Pi_a^R(\mathbf{q};\omega,t)V_{aa}} \equiv \frac{\Pi_a^R(\mathbf{q};\omega,t)}{\varepsilon_a^R(\mathbf{q};\omega,t)}, \tag{35}$$

with ε_a^R being the retarded dielectric function of the subsystem a. The imaginary parts are given by

$$V_{aa}\ \mathrm{Im}\ \mathcal{L}_a^R(\mathbf{q};\omega,t) = \mathrm{Im}\ \varepsilon_a^{R^{-1}}(\mathbf{q};\omega,t) = -\frac{\mathrm{Im}\ \varepsilon_a^R(\mathbf{q};\omega,t)}{|\varepsilon_a^R(\mathbf{q};\omega,t)|^2}. \tag{36}$$

Then, the energy-transfer rate can be written as

$$Z_{ei}(t) = -4\mathcal{V}\hbar \int \frac{d^3\mathbf{q}}{(2\pi\hbar)^3} \int_0^\infty \frac{d\omega}{2\pi} \omega \Delta N_B(\omega) \times \frac{\mathrm{Im}\ \varepsilon_e^R(\mathbf{q};\omega,t)\mathrm{Im}\ \varepsilon_i^R(\mathbf{q};\omega,t)}{|\varepsilon^R(\mathbf{q};\omega,t)|^2} \tag{37}$$

with the dielectric function of the fully coupled system

$$\varepsilon^R(\mathbf{q};\omega,t) = 1 - \sum_a V_{aa}(q)\Pi_a^R(\mathbf{q};\omega,t) \tag{38}$$

in the denominator. In this description, strong coupling described by LFCs is included in the dielectric functions both in the nominator and the denominator. The mode structure is, however, only defined by the zeros of the dielectric function of the entire system ε^R.

E. Results for the energy-transfer rates

The numerical evaluation of Eqs. (30) and (37) has been described in Ref. [40]. Figure 1 shows the results for the electron-ion energy-transfer rates applying different approaches for hot highly compressed hydrogen. In this case, the ion coupling, estimated by the classical coupling parameter $\Gamma_{ii} = (Ze)^2/(a_i k_B T_i)$ with $a_i = (3/4\pi n_i)^{1/3}$, is very high. The electrons are however mostly weakly coupled as they become degenerate at low temperatures. To include degeneracy, we define the electron coupling by replacing $\frac{3}{2}k_B T_e$ in the classical definition by the average electron kinetic energy. The highest electron coupling is thus given by the $T=0$ results at low temperatures.

In Fig. 1, we have also plotted LS rates using hyperbolic orbits [16,26]. The latter agrees with the FGR rate at high electron temperatures, but it is consistently smaller for lower

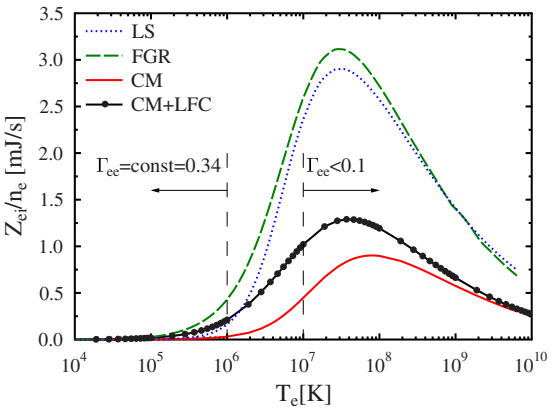

FIG. 1. (Color online) Energy-transfer rates for hydrogen plasmas with $n_e=n_i=10^{26}$ cm^{-3} and $T_i=10^4$ K in different approximations: LS as defined in Ref. [40], FGR [Eq. (27)], CM [Eq. (37)] in RPA (no LFCs), and CM including ionic LFCs according to Eq. (33). The ion coupling is $\Gamma_{ii}=191$.

temperatures as the classical approach breaks down for these cases with degenerate electrons. The CM rates with and without LFC are considerably smaller than FGR rates. The maximum lowering at lower electron temperatures is almost an order of magnitude and the high-temperature ratio is roughly one-half [40]. For the high ion coupling considered here, LFCs are quite important. In the case of Fig. 1, they result in slightly increased energy-transfer rates compared to CM rates that neglect LFC and use a dielectric function in RPA. In other cases, we find a further reduction in the rates.

IV. ENERGY AND TEMPERATURE RELAXATION

The energy relaxation in two-temperature systems can be determined via Eq. (8) using an appropriate energy-transfer rate as for instance given by formula (37). First, the species energies must be related to the temperatures via an quasiequation of state. Here, we consider two-component plasmas with temperatures T_e and T_i and ions in a single charge state Z. The total energy of each subsystem $(a=e,i)$ can be expressed by the internal energies

$$U_a(T_e,T_i)=\langle K_a\rangle+\langle V_a\rangle. \tag{39}$$

Consistent with energy-transfer rates (30) and (37), the cross contributions U_{ei} are divided evenly between the electron and ion energies. Then the energy balance equations for both subsystems [Eq. (8)] can be combined as

$$\begin{pmatrix} \frac{\partial U_e}{\partial T_e} & \frac{\partial U_e}{\partial T_i} \\ \frac{\partial U_i}{\partial T_e} & \frac{\partial U_i}{\partial T_i} \end{pmatrix} \begin{pmatrix} \frac{dT_e}{dt} \\ \frac{dT_i}{dt} \end{pmatrix} = \begin{pmatrix} Z_{ei}(T_e,T_i) \\ -Z_{ei}(T_e,T_i) \end{pmatrix}, \tag{40}$$

and one obtains for the temporal evolution of the electron and ion temperatures

$$\frac{\partial T_e}{\partial t}=\frac{Z_{ei}(T_e,T_i)}{\Delta}\left(\frac{\partial U_e}{\partial T_i}+\frac{\partial U_i}{\partial T_i}\right), \tag{41}$$

$$\frac{\partial T_i}{\partial t}=-\frac{Z_{ei}(T_e,T_i)}{\Delta}\left(\frac{\partial U_e}{\partial T_e}+\frac{\partial U_i}{\partial T_e}\right), \tag{42}$$

$$\text{with}\quad \Delta=\frac{\partial U_e}{\partial T_e}\frac{\partial U_i}{\partial T_i}-\frac{\partial U_e}{\partial T_i}\frac{\partial U_i}{\partial T_e}.$$

Energy and temperature relaxation are thus determined by the energy-transfer rates and the heat capacities of the electrons and the ions. The numerical evaluation of the energy-transfer rates was described in Sec. III (see also Ref. [40]). The next subsection will describe the calculation of the heat capacity and then we will give results for the relaxation.

A. Internal energies

The quantum behavior of the electrons and the strong-coupling effects for the ions are important properties that must be incorporated into the calculation of the internal energy and subsequently the heat capacity of the electron and ion subsystems in a dense two-temperature plasma.

In the approach presented, the electrons can be highly degenerate, partially degenerate, or classical. Moreover, correlations can change the electron heat capacity. The most accurate method to determine the heat capacity of a correlated electron gas utilizes the density of states (DOS) $g(\epsilon)$ and the Fermi function $f(\epsilon,\mu_e,T_e)$ [49]

$$\frac{\partial U_e}{\partial T_e}=\int_{-\infty}^{\infty}d\epsilon[\epsilon-\epsilon_F]\frac{\partial f(\epsilon,\mu_e,T_e)}{\partial T_e}g(\epsilon). \tag{43}$$

Here, ϵ_F is the Fermi energy and it would be required to calculate the DOS first, preferably by a first-principles simulation. This is however unfeasible for calculating a complete temperature relaxation process. Easier models for the DOS exist for the free-electron gas only. Instead, we opt to calculate the internal energy for the electrons via the Green's function technique [44]. This method makes it possible to incorporate all terms up to second order in the interaction [50],

$$U_{ee}(T_e,\mu_e)=U_e^{id}(T_e,\mu_e)+U_{ee}^{HF}(T_e,\mu_e)+U_{ee}^{MW}(T_e,\mu_e)+U_{ee}^{e^4n}(T_e,\mu_e), \tag{44}$$

$$n_e(T_e,\mu_e)=\frac{2}{\Lambda_e^3}I_{1/2}(\mu_e/k_BT_e). \tag{45}$$

Here, $\Lambda_e^2=2\pi\hbar^2/m_ek_BT_e$ is the deBroglie wavelength.

The ideal internal energy is given by

$$U_e^{id}(T_e,\mu_e)=\frac{3\mathcal{V}}{\beta\Lambda_e^3}I_{3/2}(\mu_e/k_BT_e). \tag{46}$$

The Fermi integrals I_ν are defined in Ref. [44]. Equation (46) is valid for arbitrary degeneracy including the classical and the $T=0$ limits where the heat capacities are $c_V=1.5k_B$ and $c_V\sim T$, respectively.

The higher-order terms in Eq. (44) are the Hartree-Fock (HF), Montroll-Ward (MW), and normal e^4 exchange (e^4n) terms. These terms can also be evaluated for arbitrary degeneracy [44,50,51]. The description is consistent with the ap-

proximations made for the energy-transfer rates. It is quite sufficient for laser-produced two-temperature systems with comparably hot electrons. For the cold electrons as found in shock-produced states such perturbation approach is not suitable. However, the heat capacity is only determined by the DOS at the Fermi edge for such degenerate systems, and we expect the ideal heat capacity to be a sufficient approximation.

The heat capacity of the strongly coupled ions is the main source of deviation from the ideal behavior. The ideal ion heat capacity can be very well represented by its classical value so that we can write

$$\frac{1}{N}\frac{\partial U_i}{\partial T_i} = \frac{3}{2}k_B + \frac{\partial u_i^c}{\partial T_i}. \tag{47}$$

The correlation contribution u_i^c to the internal energy of the ionic subsystem can be computed within the effective one-component model from the (temperature-dependent) pair distribution function g_{ii} via

$$u_i^c(T_i,T_e) = \frac{n_i}{2}\int_0^\infty d\mathbf{r}[g_{ii}(r;T_i,T_e)-1]\phi_{ii}(r;T_e). \tag{48}$$

The pair distribution function may be obtained via the hypernetted-chain (HNC) equation applying an effective potential ϕ_{ii} [52]. This technique allows to reasonably well represent the features of strong coupling in the ionic system [47,48]. The use of the Coulomb potential is equivalent to the FGR (uncoupled electron and ion subsystems). In first order, the effect of the electrons can be incorporated by using a linearly screened potential

$$\phi_{ii}(r;T_e) = \frac{Z^2e^2}{r}\exp[-\kappa_e(T_e)r]. \tag{49}$$

To incorporate degeneracy, the inverse screening length of the electrons has to be calculated from the electron Fermi distribution via $\kappa_e^2=(4e^2m_e/\pi\hbar^3)\int_0^\infty dp f_e(p)$.

If an effective ion-ion potential is used, electron-ion contributions are included in the internal energy of the ions. These terms can be separated by evaluating Eq. (48) for both Coulomb and effective potentials where the pair distribution has to be always calculated using an effective potential. The difference of both calculations is the cross contribution which is then distributed evenly between the electron and ion subsystem. Contributions from $\partial U_i/\partial T_e$ and $\partial U_e/\partial T_i$ arise here naturally.

B. Numerical results and discussion

The principal progression of temperature relaxation is demonstrated in Fig. 2 where an ideal noninteracting system is considered. On a scale of picoseconds, electron and ion temperatures equilibrate. The final temperature of the system with $Z=1$ is the arithmetic average of the initial electron and ion temperatures if electrons and ions obey the same statistics, i.e., Boltzmann. In the quantum case, the electron heat capacity is reduced compared to its classical value. Hence, a considerable lowering of the final equilibrium temperature occurs for the case with a quantum heat capacity.

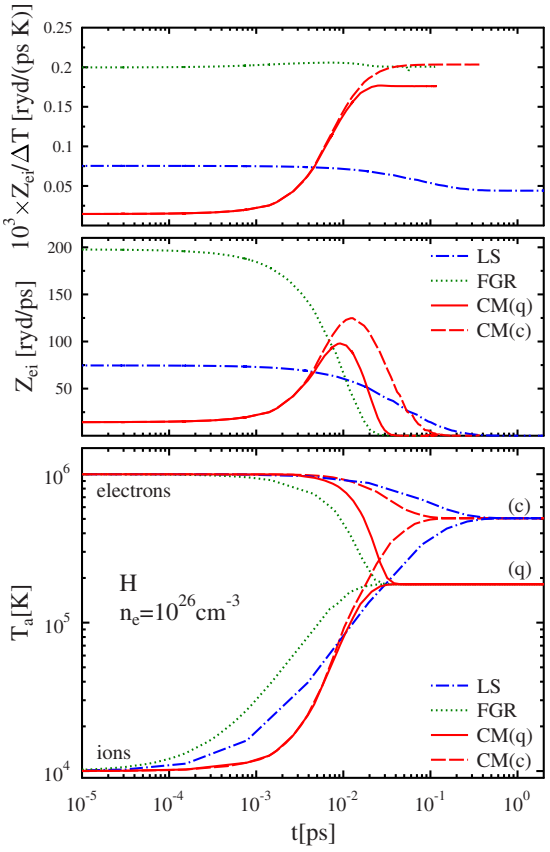

FIG. 2. (Color online) Ideal temperature relaxation in a laser-produced two-temperature hydrogen plasma. The lower panel shows the temporal evolution of the electron and the proton temperatures subject to different energy-transfer rates. The heat capacities are taken to be the ones for ideal gases in the classical limit (c) as well as the full quantum (q) expression (46). The middle panel shows the energy-transfer rates during the relaxation. For better comparison, the upper panel shows rates normalized by the temperature difference.

The final plasma temperature depends only on the quasi-equation of state, that is, heat capacities (44) and (47) of the subsystems. It is independent of the energy-transfer rate. The energy-transfer rates, on the other hand, govern the evolution of the temperatures and the relaxation time. Figure 2 compares different approaches for the energy-transfer rates. The LS transfer rate [16,26] gives the longest equilibration time. We restrict us here to classical heat capacities as the LS rate was derived in a purely classical framework. Comparing the result of the LS relaxation with the relaxation on the basis of the CM rate, one observes that the CM relaxation time is smaller by roughly a factor of 5. This is even more surprising when noting that during the first stages of the relaxation CM rates are lower than LS rates and consequently a very slow equilibration is predicted. However, the CM relaxation accelerates for small temperature differences relative to the LS equilibration and finally results in a shorter total relaxation time.

There are three reasons for this behavior. First, the larger temperature difference in the CM case between 10^{-4} and 10^{-2} ps will eventually drive increased energy transfer as

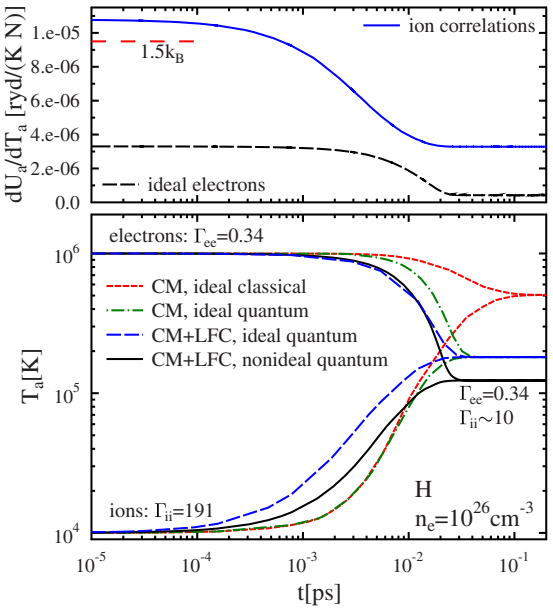

FIG. 3. (Color online) Nonideal temperature relaxation in a hydrogen plasma. The lower panel shows electron and ion temperatures following from different energy-transfer rates and heat capacities. The upper panel shows contributions to the heat capacity as included in the black solid curve: ideal heat capacities for both species and correlation contribution to the heat capacity of the ions according to Eq. (48).

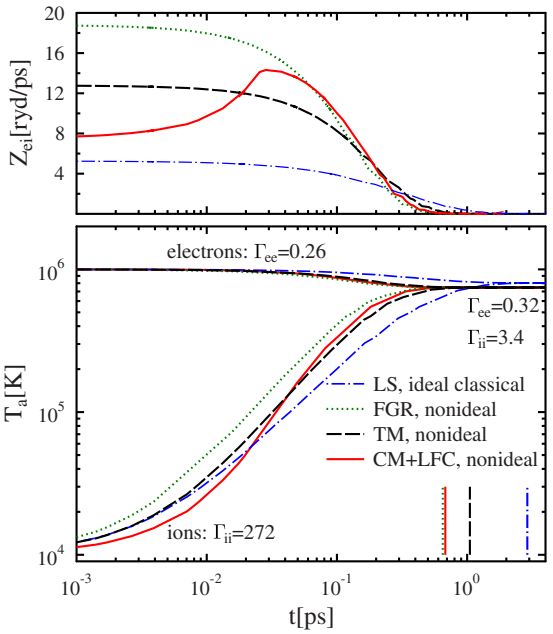

FIG. 4. (Color online) Nonideal temperature relaxation in a beryllium plasma with $Z=4$, $n_e=10^{24}$ cm^{-3}, $T_e(0)=10^6$ K, and $T_i(0)=10^4$ K. The vertical lines indicate the relaxation times for the different energy-transfer rates: T-matrix (TM) [22], FGR [Eq. (27)], and CM+LFC [Eq. (37)]. All lines except LS include ionic correlations in the heat capacity.

$Z_{ei}\sim T_e-T_i$. Second, the coupled-mode effect, that considerably reduces energy transfer, exists only for large temperature differences and is negligible for later times (see upper panel in Fig. 2) [40]. Third and most importantly, the approximations for the LS energy-transfer rates break down, yielding too low LS rates (see Fig. 1 and Refs. [22,40]).

Let us now compare results based on expressions which were quantum statistically derived and thus justify the use of the quantum heat capacity for the electrons. The FGR rates are highest and consequently predict the fastest relaxation. The CM rates on the basis of the RPA dielectric function are the smallest leading to the longest relaxation time. Furthermore, the CM rate does not merge with the FGR rate in the quantum case when approaching equilibrium as the electrons are highly degenerate. This behavior occurs as the Fermi temperature defines the mode spectrum in this case and ion acoustic modes, which reduce the rates, exist even for $T_i \approx T_e$. Moreover, strongly coupled ions have to be considered here. Including LFC into the rates predicts a relaxation only slightly longer than FGR (not shown).

Figure 3 demonstrates the influence of strong coupling in the energy-transfer rates and the heat capacities. The nonideality contributions to the electron and ion heat capacities were calculated as described in Sec. IV A. Together with the consideration of LFC according to Eq. (33) in the CM energy-transfer rate, this results in a consistent description of the equilibration process. Not only kinetic energy is transferred but potential energy serves as heat source or sink that considerably influences the final temperature, the relaxation time, and the shape of the temperature evolution.

For comparison, we show an ideal relaxation using the CM rate and classical heat capacity again. When using the correct quantum heat capacity for the electrons, the final temperature is lowered by a factor of 2.7 and the relaxation time is decreased by a factor of 3. LFCs in the CM rates increase the speed of the relaxation slightly, but correlations in the heat capacity of the ions further decrease the final temperature by a factor of 1.5. There is only a marginal change in the relaxation time due to the inclusion of potential-energy contributions to the heat capacity, but the latter strongly influence the course of the relaxation.

It is also interesting to study the time-dependent heat capacities of electrons and ions as they drive or delay the relaxation. The upper panel of Fig. 3 provides those quantities. Compared to a classical ideal gas, the ideal quantum heat capacity of the electrons is reduced by more than a factor of 3. In the course of relaxation, the ideal electron heat capacity further decreases with electron temperature as the electrons become more degenerate. Correlation contributions to the electron heat capacity are of the order of -10^{-7} ryd/(KN). This means that they tend to decrease the electron heat capacity but they are negligible here. The heat capacity of the ions comprises the ideal part ($1.5k_B$) and the correlation contribution which is of the same order. This leads to an ion heat capacity that is almost an order of magnitude larger than the electron heat capacity. Similar to the electron heat capacity, the ion heat capacity becomes smaller with time. However, this is due to reduced coupling strength and, thus, a reduced nonideality contribution as the ion temperature increases.

We now turn to heavier elements which allow higher charge states. As the first example, we choose beryllium under laser-heated conditions. Figure 4 contains results of our calculations for the nonideal relaxation. In this case, there is

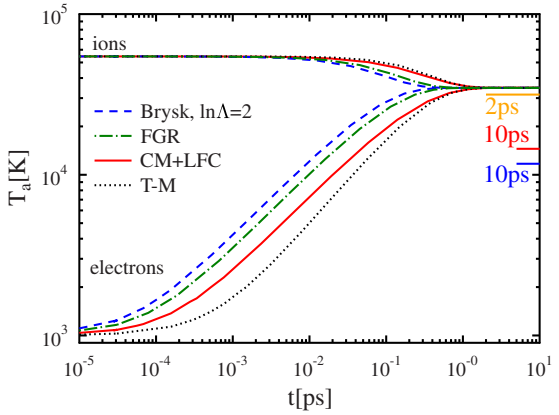

FIG. 5. (Color online) Nonideal temperature relaxation in a silicon plasma with $Z=4$ and $n_e=5.36\times10^{23}$ cm^{-3} [20]. All relaxation shown include the quantum heat capacity for the electrons and correlations for the ion heat capacity while using different energy-transfer rates: Brysk [53], TM [22], FGR [Eq. (27)], CM+LFC [Eq. (37)]. The short lines and times at the right indicate the final temperatures and relaxation times in three simplified cases: CM+LFC energy-transfer rates and (i) an ideal classical relaxation (lowest), (ii) quantum electrons and correlations in the ion heat capacity included (middle), and (iii) ideal relaxation with quantum heat capacity of the electrons (highest).

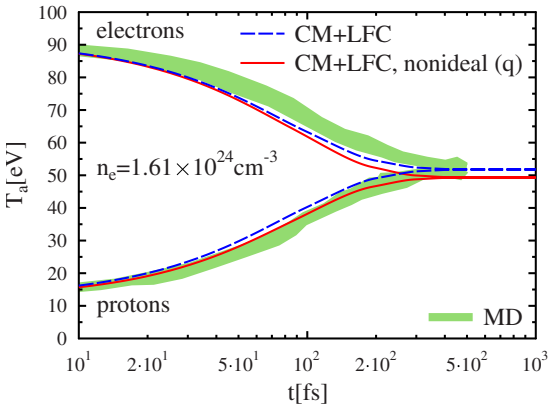

FIG. 6. (Color online) Temperature relaxation in a hydrogen plasma. Shown are the MD results from Glosli *et al.* [41] and our calculations using CM energy-transfer rates [Eq. (37)]. The initial electron and proton temperatures are $T_e=91.47$ eV and $T_p=12.1$ eV, respectively. The dashed curve is for an ideal, classical relaxation and the solid curve includes ionic correlations in the heat capacity and quantum electrons.

only a difference of 0.6% between calculations using a quantum or a classical heat capacity. Different from hydrogen, the final temperature is very close to the initial electron temperature as the electron density is four times higher than the ion density. Ionic correlations lower the final temperature by 7%. The most important effect of the ionic correlations in the heat capacity is the evolution of the ion temperature. It takes considerably longer to heat up correlated ions (0.2 ps difference between cases with and without ionic correlations). The final relaxation time is thus longer if correlations are included (here, by a factor of 1.4). Interestingly, the fact that the CM energy-transfer rates are lower than FGR and T-matrix rates during the initial phase does not lead to considerably longer relaxation times. CM and FGR rates merge when the temperature difference is too small for ion acoustic modes to exist [40]. Since the FGR rates are higher than the T-matrix rates for all times (FGR is a first Born approximation only), the T-matrix calculation displays the longest relaxation time of all quantum approaches. Still, the LS approach predicts a relaxation that lasts at least a factor of 3 longer.

Finally, we analyze a shock-produced two-temperature plasma. The experimental conditions of Ng *et al.* [20] provide an interesting case as the measured relaxation times were orders of magnitude larger than expected. In this case, the electrons are highly degenerate and the usual LS approach completely breaks. Instead, we show results of the Brysk energy-transfer rate [53] with a clamped Coulomb logarithm in Fig. 5. This approach has the shortest relaxation time. FGR rates give slightly longer equilibration times. The relaxation times from the CM+LFC and T-matrix approaches are similar around 1 ps. It should be however stressed that the fit to the T-matrix calculation is here overstretched.

The deviation in the final temperature from an ideal classical case, which yields $T=12\,625$ K, is largely due to the low heat capacity of the degenerate electrons. Ionic correlations in the heat capacity account for a 15% deviation from ideal behavior. This is also the reason why the full calculations in Fig. 5 show shorter relaxation times than the ideal or classical results. Correlations in the ionic subsystem increase the ion heat capacity and slow the relaxation down. However, the quantum effects of the electrons dominate and the decrease in the electron heat capacity accelerates the relaxation.

Recently Glosli *et al.* published MD results for the temperature equilibration process [41]. Figure 6 contains the relaxation of the electron and ion temperatures as seen in their MD simulation and as it was calculated with the theory presented here. The agreement between an ideal classical relaxation with CM+LFC rates and the MD simulation is rather good. It is in fact better than using any other approach for the energy-transfer rate at our disposal. If we apply the LS formula with hyperbolic orbits [22], we find relaxation times that are a factor of 2 longer than the MD shows. This fact together with the observation of Glosli *et al.*, that their LS rates predict a relaxation two times faster than MD, clearly prohibit the application of any LS approach.

Still, we can clearly distinguish between a classical ideal relaxation and a more realistic nonideal case with the electrons being described quantum statistically. The resulting relaxation time does not change significantly as electron quantum effects and ionic correlations have an opposite influence. However, the final temperature is lowered by 3% due to quantum electrons. Of course, this cannot be picked up by classical MD simulations.

V. CONCLUSION

Based on a quantum statistical theory of plasmas, we have presented a rigorous derivation of balance equations for the energy relaxation in two-temperature plasmas. Within this approach, quantum exchange and potential-energy contribu-

tions to the internal energy are included naturally. Moreover, the division problem of cross species correlations is solved. Our approach yields a very general expression for the energy-transfer rate that is consistent with the internal energy used. The well-known FGR and CM energy-transfer rates follow from this general form as approximations. The present CM scheme generalizes the expression obtained from kinetic theory based on the Lenard-Balescu equation [40] as it also contains strong-coupling effects. Moreover, our derivation highlights the approximations that are inherent to the present CM description: the cross terms in the polarization function are neglected and the gradient expansion with respect to the macroscopic time t is considered in lowest order.

The numerical evaluation of the FGR and CM rates reveals the importance of electron degeneracy and strong coupling. Both influence the occurrence of ion acoustic modes and thus can trigger large differences between the FGR and CM rates. Strong correlations, described by static LFCs, can further change the dispersion relation and the width of these modes which leads to significant changes for plasmas with strongly coupled ions. The rates normalized by the temperature difference, $T_e - T_i$, (known as energy coupling constants) are indeed almost constant if described within the LS, FGR, or T-matrix approach while the CM energy coupling constants may change considerably during the relaxation.

The equilibration process is also strongly influenced by potential-energy contributions. Our approach allows for a consistent description of the heat capacities and energy-transfer rates including strong correlations and exchange. Ionic properties have been described via classical integral equation techniques. Contributions of the electrons have been calculated using a quantum perturbation approach. The relaxation times in highly degenerate plasmas are significantly shorter than a classical description predicts. Contributions of ionic correlations in the internal energy tend to increase the relaxation times, but they mainly affect the final temperature and the evolution of the ion temperature. Our comparison with recent classical MD simulations shows reasonable agreement if the CM energy-transfer rates are used.

For future applications and comparisons, we favor CM rates including LFC combined with a consistent set of heat capacities. However, strong electron-ion scattering (T-matrix) effects should be included in addition to yield a more realistic and truly superior description.

ACKNOWLEDGMENTS

This work was supported by the U.K.'s Engineering and Physical Sciences Research Council (Grant No. EP/D062837) and the Deutsche Forschungsgemeinschaft (SFB 652).

APPENDIX: GENERAL EXPRESSIONS FOR THE ENERGY-TRANSFER RATE

We start with the expression for energy-transfer rate (11) and insert relation (13) to obtain

$$Z_{ab} = \frac{1}{2i\hbar}\mathrm{Tr}_{1,2}\{(\hat{H}_a - \hat{H}_b)[\hat{V}_{ab}, \hat{\rho}_a\hat{\rho}_b + i\hbar L_{ab}^{<}]\}. \tag{A1}$$

By applying the equations of motion for the creation and annihilation operators [44], one can derive the following equations of motion for the function $L_{ab}^{<}(t_1,t_2)$:

$$i\hbar\frac{\partial}{\partial t_1}L_{ab}^{<}(t_1,t_2) = [\hat{H}_a, L_{ab}^{<}(t_1,t_2)] + i\hbar\sum_c \mathrm{Tr}_3[\hat{V}_{ac}, L_{(ac)b}^{<}(t_1,t_2)],$$

$$i\hbar\frac{\partial}{\partial t_2}L_{ab}^{<}(t_1,t_2) = [\hat{H}_b, L_{ab}^{<}(t_1,t_2)] + i\hbar\sum_c \mathrm{Tr}_3[\hat{V}_{bc}, L_{a(bc)}^{<}(t_1,t_2)], \tag{A2}$$

where the special three-particle correlation functions are given by

$$(i\hbar)^2 L_{(ac)b}^{<}(t_1,t_2) = \langle\psi_b^\dagger(t_2)\psi_b(t_2)\psi_a^\dagger(t_1)\psi_c^\dagger(t_1)\psi_c(t_1)\psi_a(t_1)\rangle - \langle\psi_b^\dagger(t_2)\psi_b(t_2)\rangle\langle\psi_a^\dagger(t_1)\psi_c^\dagger(t_1)\psi_c(t_1)\psi_a(t_1)\rangle \tag{A3}$$

and

$$(i\hbar)^2 L_{a(bc)}^{<}(t_1,t_2) = \langle\psi_b^\dagger(t_2)\psi_c^\dagger(t_2)\psi_c(t_2)\psi_b(t_2)\psi_a^\dagger(t_1)\psi_a(t_1)\rangle - \langle\psi_b^\dagger(t_2)\psi_c^\dagger(t_2)\psi_c(t_2)\psi_b(t_2)\rangle\langle\psi_a^\dagger(t_1)\psi_a(t_1)\rangle. \tag{A4}$$

The expression on the right-hand side of Eq. (A1) can be transformed with help of Eq. (13) and the equations of motion [Eq. (A2)] into the form

$$\begin{aligned} Z_{ab} = {} & \frac{1}{2}\mathrm{Tr}_{1,2}\frac{1}{i\hbar}\{(\hat{H}_a - \hat{H}_b)[\hat{V}_{ab}, \hat{\rho}_a\hat{\rho}_b]\} \\ & + \frac{1}{2}\mathrm{Tr}_{1,2}\, i\hbar\hat{V}_{ab}\left\{\left(\frac{\partial}{\partial t_2} - \frac{\partial}{\partial t_1}\right)L_{ab}^{<}(t_1,t_2)\right\}\Big|_{t_1=t_2} \\ & - \frac{1}{2}\sum_c \mathrm{Tr}_{1,2,3}\, i\hbar\hat{V}_{ab}\{[\hat{V}_{ac}, L_{a(bc)}^{<}(t_1,t_1)] \\ & - [\hat{V}_{bc}, L_{(ac)b}^{<}(t_1,t_1)]\}. \end{aligned} \tag{A5}$$

Using the equal-time commutation relations for the field operators and accounting for $b \neq a$, we have

$$(i\hbar)^2 L_{a(bc)}^{<}(t_1,t_1) = \delta_{ac}\delta(3-1')\langle\psi_a^\dagger(1')\psi_b^\dagger(2')\psi_c(3)\psi_a(1)\rangle + \hat{\rho}_{abc}(t_1) - \hat{\rho}_a(t_1)\hat{\rho}_{bc}(t_1), \tag{A6}$$

where $\hat{\rho}_{abc}$, $\hat{\rho}_{bc}$, and $\hat{\rho}_a$ denote three-, two-, and one-particle density matrices, respectively. By inserting this relation and a similar one for $L_{(ac)b}^{<}(t_1,t_1)$ into Eq. (A5), one can see easily that some terms vanish or cancel each other. Then we find using the equation of motion for the one-particle density operator

$$Z_{ab} = \frac{1}{2}\mathrm{Tr}_{1,2}\, i\hbar V_{ab} \left\{ \left(\frac{\partial}{\partial t_2} - \frac{\partial}{\partial t_1} \right) L_{ab}^{<}(t_1,t_2) \right\} \Bigg|_{t_1=t_2} + \frac{1}{2}\mathrm{Tr}_{1,2}\, V_{ab} \left\{ \rho_a \left(\frac{\partial}{\partial t_1}\rho_b \right) - \left(\frac{\partial}{\partial t_1}\rho_a \right)\rho_b \right\}. \quad \text{(A7)}$$

The second term on the rhs vanishes for spatially homogeneous systems. In the first term, we can introduce the Fourier transform of the correlation function of density fluctuations $L_{ab}^{<}(t_1,t_2)$ with respect to the time difference $\tau = t_1 - t_2$ defined by

$$L_{ab}^{<}(\tau,t) = \int \frac{d\omega}{2\pi} e^{-i\omega\tau} L_{ab}^{<}(\omega,t), \quad \text{(A8)}$$

where $t = \frac{1}{2}(t_1+t_2)$ is the macroscopic time. Then we get for the energy-transfer rate

$$Z_{ab} = -\mathrm{Tr}_{1,2} \int_{-\infty}^{\infty} \frac{d\omega}{2\pi} \hbar\omega \hat{V}_{ab} L_{ab}^{<}(\omega,t). \quad \text{(A9)}$$

[1] A. Ravasio *et al.*, Phys. Rev. Lett. **99**, 135006 (2007).
[2] S. H. Glenzer *et al.*, Phys. Rev. Lett. **98**, 065002 (2007).
[3] E. García Saiz *et al.*, Nat. Phys. **4**, 940 (2008).
[4] A. L. Kritcher *et al.*, Science **322**, 69 (2008).
[5] B. Barbrel *et al.*, Phys. Rev. Lett. **102**, 165004 (2009).
[6] G. W. Collins *et al.*, Science **281**, 1178 (1998).
[7] M. D. Knudson, D. L. Hanson, J. E. Bailey, C. A. Hall, J. R. Asay, and W. W. Anderson, Phys. Rev. Lett. **87**, 225501 (2001).
[8] R. F. Smith, J. H. Eggert, M. D. Saculla, A. F. Jankowski, M. Bastea, D. G. Hicks, and G. W. Collins, Phys. Rev. Lett. **101**, 065701 (2008).
[9] A. Grinenko, D. O. Gericke, and D. Varensov, Laser and Part. Beams **27**, 595 (2009).
[10] J. D. Lindl *et al.*, Phys. Plasmas **11**, 339 (2004).
[11] B. Militzer, W. B. Hubbard, J. Vorberger, I. Tamblyn, and S. A. Bonev, Astrophys. J. Lett. **688**, L45 (2008).
[12] N. Nettelmann *et al.*, Astrophys. J. **683**, 1217 (2008).
[13] A. L. Kritcher *et al.*, Phys. Rev. Lett. **103**, 245004 (2009).
[14] M. W. C. Dharma-wardana and F. Perrot, Phys. Rev. E **58**, 3705 (1998).
[15] L. D. Landau, Phys. Z. Sowjetunion **10**, 154 (1936).
[16] L. Spitzer, *Physics of Fully Ionized Gases* (Interscience, New York, 1962).
[17] J. P. Hansen and I. R. McDonald, Phys. Lett. A **97**, 42 (1983).
[18] U. Reimann and C. Toepffer, Laser Part. Beams **8**, 763 (1990).
[19] P. Celliers, A. Ng, G. Xu, and A. Forsman, Phys. Rev. Lett. **68**, 2305 (1992).
[20] A. Ng, P. Celliers, G. Xu, and A. Forsman, Phys. Rev. E **52**, 4299 (1995).
[21] D. Riley, N. C. Woolsey, D. McSherry, I. Weaver, A. Djaoui, and E. Nardi, Phys. Rev. Lett. **84**, 1704 (2000).
[22] D. O. Gericke, M. S. Murillo, and M. Schlanges, Phys. Rev. E **65**, 036418 (2002).
[23] D. O. Gericke, M. S. Murillo, and M. Schlanges, Laser Part. Beams **20**, 543 (2002).
[24] Note that a classical collision theory yields for dense plasmas too low and with further increasing density (or decreasing temperature) negative Coulomb logarithms which translates into too low or negative energy-transfer rates in the Landau-Spitzer theory. The consideration of hyperbolic orbits [22] avoids the total break down of the theory for high densities (low temperatures), but it still underestimates the cross sections.
[25] G. Hazak, Z. Zinamon, Y. Rosenfeld, and M. W. C. Dharma-wardana, Phys. Rev. E **64**, 066411 (2001).
[26] D. O. Gericke, J. Phys.: Conf. Ser. **11**, 111 (2005).
[27] M. E. Kim, A. Das, and S. D. Senturia, Phys. Rev. B **18**, 6890 (1978).
[28] M. W. C. Dharma-wardana, Phys. Rev. Lett. **66**, 197 (1991).
[29] D. O. Gericke and M. S. Murillo, *Proceedings of the International Conference. on Inertial Fusion Science and Applications Monterey*, edited by W. J. Hogan (American Nuclear Society, La Grange Park, IL, 2004).
[30] D. O. Gericke, M. S. Murillo, D. Semkat, M. Bonitz, and D. Kremp, J. Phys. A **36**, 6087 (2003).
[31] D. O. Gericke, Th. Bornath, and M. Schlanges, J. Phys. A **39**, 4739 (2006).
[32] J. Daligault and G. Dimonte, Phys. Rev. E **79**, 056403 (2009).
[33] Th. Ohde, M. Bonitz, Th. Bornath, D. Kremp, and M. Schlanges, Phys. Plasmas **3**, 1241 (1996).
[34] Th. Bornath, M. Schlanges, and R. Prenzel, Phys. Plasmas **5**, 1485 (1998).
[35] D. O. Gericke, G. K. Grubert, Th. Bornath, and M. Schlanges, J. Phys. A **39**, 4727 (2006).
[36] M. W. C. Dharma-wardana, Phys. Rev. E **64**, 035401(R) (2001).
[37] J. Daligault and D. Mozyrsky, Phys. Rev. E **75**, 026402 (2007).
[38] J. Daligault and D. Mozyrsky, High Energy Density Phys. **4**, 58 (2008).
[39] G. Gregori and D. O. Gericke, EPL **83**, 15002 (2008).
[40] J. Vorberger and D. O. Gericke, Phys. Plasmas **16**, 082702 (2009).
[41] J. N. Glosli, F. R. Graziani, R. M. More, M. S. Murillo, F. H. Streitz, M. P. Surh, L. X. Benedict, S. Hau-Riege, A. B. Langdon, and R. A. London, Phys. Rev. E **78**, 025401(R) (2008).
[42] W.-D. Kraeft, D. Kremp, W. Ebeling, and G. Röpke, *Quantum Statistics of Charged Particle Systems* (Akademie-Verlag, Berlin, 1986).
[43] V. L. Keldysh, Zh. Eksp. Teor. Fiz. **47**, 1515 (1964) [Sov. Phys. JETP **20**, 235 (1965)].
[44] D. Kremp, M. Schlanges, and W.-D. Kraeft, *Quantum Statistics of Nonideal Plasmas* (Springer-Verlag, Berlin, Heidelberg, 2005).
[45] D. C. Langreth and J. W. Wilkins, Phys. Rev. B **6**, 3189 (1972).
[46] S. Ichimaru, Rev. Mod. Phys. **54**, 1017 (1982).
[47] K. Wünsch, P. Hilse, M. Schlanges, and D. O. Gericke, Phys. Rev. E **77**, 056404 (2008).
[48] K. Wünsch, J. Vorberger, and D. O. Gericke, Phys. Rev. E **79**,

010201(R) (2009).
[49] N. W. Ashcroft and N. D. Mermin, *Solid State Physics* (Holt, Rinehart, Winston, New York, 1976).
[50] J. Vorberger, M. Schlanges, and W.-D. Kraeft, Phys. Rev. E **69**, 046407 (2004).
[51] W.-D. Kraeft, M. Schlanges, J. Vorberger, and H. E. DeWitt, Phys. Rev. E **66**, 046405 (2002).
[52] J. F. Springer, M. A. Pokrant, and F. A. Stevens, Jr., J. Chem. Phys. **58**, 4863 (1973).
[53] H. Brysk, Plasma Phys. **16**, 927 (1974).